ACS APPLIED ENERGY MATERIALS

www.acsaem.org Article

Long-Term Autonomic Thermoregulating Fabrics Based on Microencapsulated Phase Change Materials

Paula F. De Castro, Sergiy Minko, Vladimir Vinokurov, Kirill Cherednichenko, and Dmitry G. Shchukin*

Cite This: *ACS Appl. Energy Mater.* 2021, 4, 12789−12797 Read Online

ACCESS | Metrics & More | Article Recommendations | Supporting Information

ABSTRACT: Microcapsules loaded with n-docosane as phase change material (mPCMs) for thermal energy storage with a phase change transition temperature in the range of 36−45 °C have been employed to impregnate cotton fabrics. Fabrics impregnated with 8 wt % of mPCMs provided 11 °C of temperature buffering effect during heating. On the cooling step, impregnated fabrics demonstrated 6 °C temperature increase for over 100 cycles of switching on/off of the heating source. Similar thermoregulating performance was observed for impregnated fabrics stored for 4 years (1500 days) at room temperature. Temperature buffering effect increased to 14 °C during heating cycle and temperature increase effect reached 9 °C during cooling cycle in the aged fabric composites. Both effects remained stable in aged fabrics for more than 100 heating/cooling cycles. Our study demonstrates high potential use of the microencapsulated n-docosane for thermal management applications, including high-technical textiles, footwear materials, and building thermoregulating covers and paints with high potential for commercial applications.

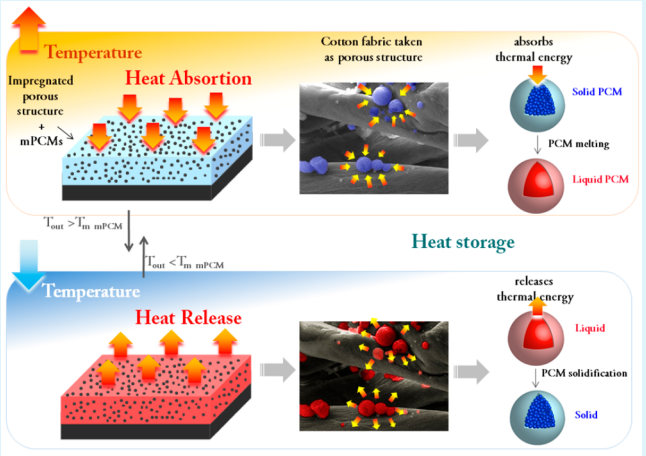

KEYWORDS: *phase change materials, encapsulation, thermal energy storage, textile materials, capsules*

1. INTRODUCTION

Phase change materials, PCMs, are materials that absorb and release thermal energy when undergoing and/or overpassing their phase change transition temperature. They attracted attention because of their potential use as thermal energy storage materials and have found niche in applications such as heat recovery, solar energy storage,[1] intelligent and energy efficient building materials, air conditioning, and photovoltaics devices[2−4] with a common goal of contributing to more efficient and environmentally friendly energy use. PCMs with solid−liquid phase change are the most practical in terms of latent heat capacity and design of the heat storage device.[5] They work in such a way that when the temperature reaches the melting temperature (T_m), the PCM absorbs the equivalent heat for melting. Reversely, when the temperature drops the PCM starts crystallizing at crystallization temperature (T_c) and releases back the heat that was previously stored.[6−8] Successful PCMs use and implementation require them to be encapsulated in order to (1) confine the liquid phase during the solid−liquid phase transition, (2) prevent their degradation when exposed to the outside environment, (3) enhance heat transfer, (4) avoid supercooling problems, and (5) improve their handling and flexibility of incorporation into different matrices without losing the functional and original properties of both PCMs and the matrices in which PCMs are incorporated.[5,9−12] Mechanical properties of the microencapsulated PCMs (mPCMs) play an important role since the shell needs to be flexible enough to overcome the volume changes during the solid−liquid transition but also be resistant against cracking to cope with the processes during their integration into the heat storage macroscale systems. Most of mPCMs had melamine−formaldehyde (MF) and urea−formaldehyde (UF),[13−17] poly(methyl methacrylate) (PMMA),[18,19] polystyrene (PS),[20,21] silica-based-[22,23] and silica shells.[24,25] The selection of the core PCM depends mainly on the temperature range and application area. Organic PCMs have been studied and used for many applications because of their high latent heat capacities, noncorrosiveness, nontoxicity, and large melting temperature range. Among them, n-octadecane, n-hexadecane, and n-eicosane have been in the focus of many studies because of their phase change

Received: August 16, 2021
Accepted: October 18, 2021
Published: October 29, 2021

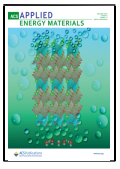

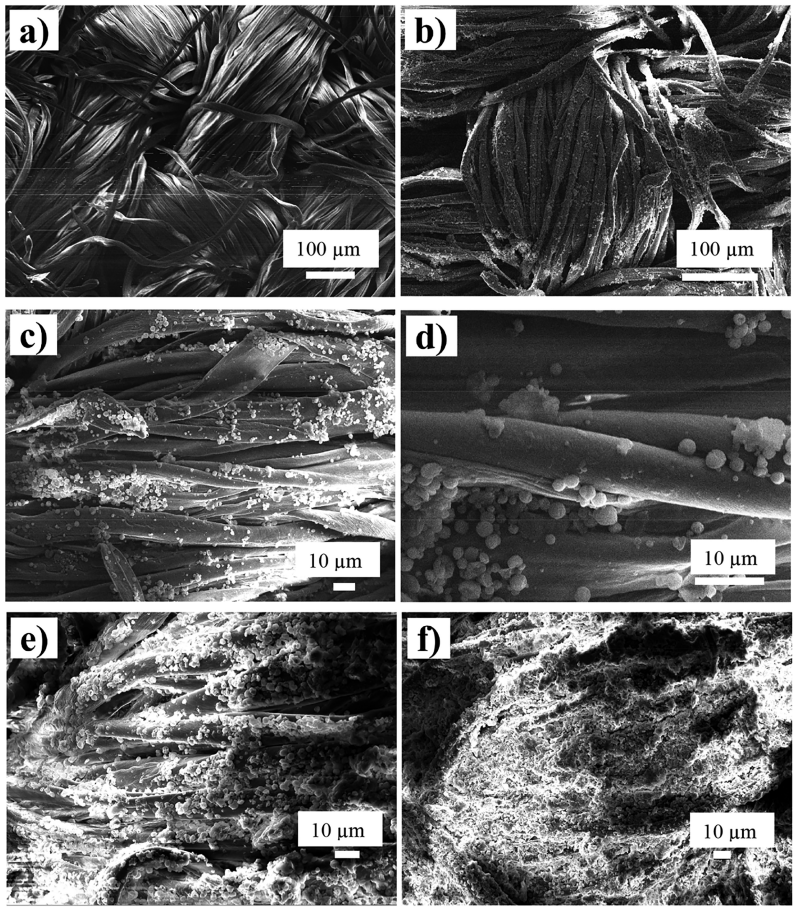

Figure 1. SEM images of the (a) cotton fabric and (b–d) 2 wt % mPCMs incorporated into fabrics at different magnifications, and (e) 8 wt % mPCMs and (f) 34 wt % of mPCMs.

temperature of about 28 °C, 36 °C, and 18 °C, which are convenient for targeting human comfort temperature.[26−29] However, these temperature ranges are lower when targeting thermoregulatory response in footwear materials, high-technical textiles, and building materials where temperature may go above 37 °C. In this study, we have prepared polyurethane (PU) microcapsules of ∼2 μm size loaded with n-docosane by the improved methodology previously developed by us[30,31] with a phase change transition in the range of 40−45 °C and incorporated them into fabrics in order to show long-term thermal buffering effect of the microcapsules which has not been reported yet. Incorporation of phase change materials into textile has been previously demonstrated for melamine formaldehyde capsules,[32] polystyrene capsules[33] and capsules with SiO_2 shell.[34−36] However, all papers previously mentioned do not demonstrate long-term heat uptake/release stability of the capsules and composites and present DSC data for first heat uptake/release cycle. The main novelty of our research is the long-term cycling stability of individual capsules during at least 100 heat uptake/release cycles as well thermal properties of composite textile materials by TGA, DSC, and FLIR measurements even after 4 years (1500 days) of the aging of thermotextiles based on microencapsulated PCMs. In addition, we show the long-term thermal buffering effect that mPCMs provide to the hosting matrices by carrying out time-dependent temperature measurements.

2. RESULTS AND DISCUSSION

Figure 1 shows SEM images of the untreated fabrics (Figure 1a) and the fabrics impregnated with mPCMs (Figures 1b–f). Fabrics were first impregnated with 2 wt % of mPCMs to study compatibility between cotton and mPCMs and then the mPCMs content was increased to 8 wt % and further to 34 wt % to explore heat self-regulation efficiency. Figure 1c–f shows mPCMs attached to the cotton surface and located between the fibers and on the fiber surface. Figure 1e demonstrates SEM images of the fabrics loaded with 8 wt % of mPCM. Well-dispersed capsules are seen along the surface of the cotton filaments. The textile fibers with 34 wt % of mPCMs in Figure 1f have a thick microcapsule coating with a high content of microcapsules in the fabrics. Figure S1 (see Supporting Information) shows a comparative images of the fabrics at different impregnation rate. Impregnation of the fabrics with mPCMs leads to an increase in the rigidity of the material that is visually observed at the corners of the specimens which are slightly bent inward. Optical microscope images of untreated fabric (Figure S2a) and treated fabric with 8 and 34 wt % of mPCMs (see Figure S2b,c, respectively) also show a higher impregnation level of the textile at higher mPCMs content. The adhesion stability of PCM capsules is demonstrated in . Capsules remain stable on the fabric surface after 24 h of exposure in a water bath at 22 °C. No weight loss has been found for composite thermoregulating textile after water treatment.

https://doi.org/10.1021/acsaem.1c02170
ACS Appl. Energy Mater. 2021, 4, 12789−12797

Characteristic mPCMs peaks[30] appear in the FTIR spectra of the impregnated fabrics (Figure 2) and their intensity

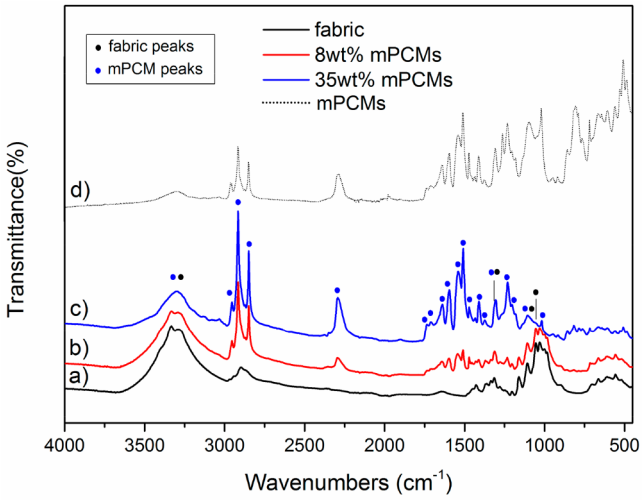

Figure 2. FTIR spectra of fabrics where (a) untreated fabric, (b) fabric with 8 wt % mPCMs, (c) fabric with 34 wt %, and (d) mPCMs.

increases when comparing fabrics with 8 and 34 wt % loading. These peaks are asymmetric and symmetric stretching vibrations of the −CH from methylene group at 2952 and 2915 cm^{-1}; stretching vibration of the −NCO appears at 2295 cm^{-1}; stretching vibration of free and bonded urethane groups (−CO) at 1732 and 1709 cm^{-1}, respectively; stretching vibration of the aromatic ring of the shell (−C═C) at 1594 cm^{-1}, peak corresponding to the −CO amide region at 1541 cm^{-1}, stretching vibration of −CN and deformation of $-NH_{assoc}$), 1509 cm^{-1}, 1471 cm^{-1}; asymmetric deformation of the $-CH_3$ at 1411 cm^{-1}; deformation of the NH_{assoc} and stretching vibration of the −CN at 1305 cm^{-1}; and the peak that corresponds to the rocking vibration of the methylene group at 717 cm^{-1}. At the same time, peaks corresponding to the fabrics decrease: bending vibration of the −OH from the carboxylic acid radicals at 3400−2400 cm^{-1}; stretching vibration of the −CH of the aldehydes that appear in the range of 2850−2750 cm^{-1}; −CH bending at 1369 cm^{-1}; −OH in-plane bending at 1335 cm^{-1}; −CH wagging at 1314 cm^{-1}; and the stretching vibrations from −CO at 1300−1101 cm^{-1}. The difference between peaks in impregnated structure comparing to initial fabric and mPCM within the 1250−750 cm^{-1} range is associated with the interaction between OH and CO groups of fabric and CN and NH group of mPCM shell stabilizing microcapsules inside fabric network.

Melting tests were visually done to determine the stability of the impregnated fabrics. Selected fabrics impregnated with 34 wt % of mPCMs and a reference prepared by impregnating 34 wt % of pure n-docosane were heated above 50 °C for 30 min and then cooled down to room temperature. The impregnated structures with mPCMs (encapsulated n-docosane) demonstrate a remarkable stability compared to those ones with directly immobilized n-docosane. As it is shown in Figure 3a,b, the initial appearance of the impregnated fabrics with 34 wt % mPCMs remains stable while, as depicted in Figure 3d, fabrics treated with pure n-docosane show the release of n-docosane from textile matrix.

Thermal stability of the thermocontrolled fabrics was also examined by thermal gravimetric analysis (TGA) (Figure 4). The untreated fabric shows weight increase of 5.4 wt % at about 86.7−326 °C due to moisture adsorption from air. The first main decomposition step takes place at about 326−345.2 °C with a weight loss of 74.5 wt % followed by the second step that occurs in the temperature range of 345.2−486.3 °C with 26 wt % weight loss, which is the result of thermal degradation and oxidation of untreated fabric below 320 °C in air. Microcapsules, mPCMs, have two main decomposition steps. The first one occurs in the range of 239.7−270 °C which involves a weight loss of 48.6 wt % related to the decomposition of the capsule shell followed by the second one that takes place at about 270−561.5 °C with a total weight loss of 49.7 wt % related to the decomposition of encapsulated

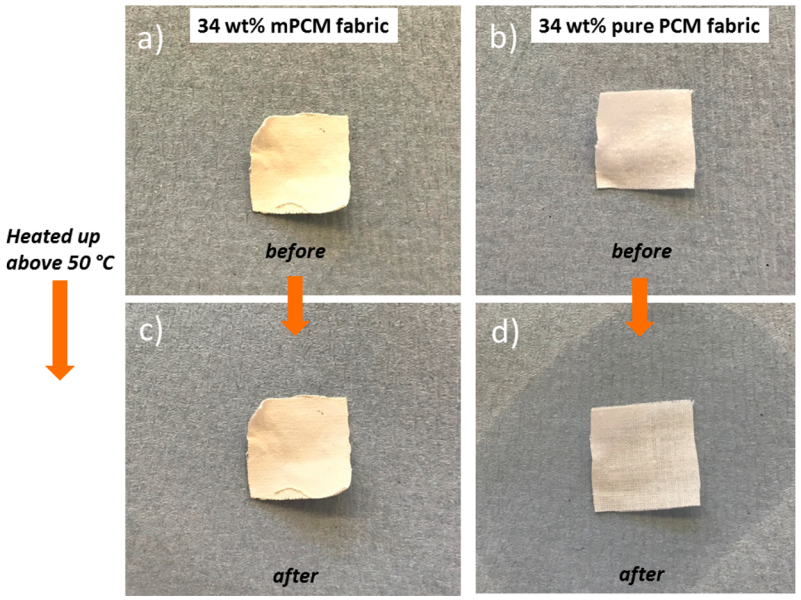

Figure 3. Images of fabric with 34 wt % mPCMs (a) before and (c) after being heated above 50 °C, and of the fabrics with 34 wt % of pure n-docosane (b) before and (d) after being heated to 50 °C.

https://doi.org/10.1021/acsaem.1c02170
ACS Appl. Energy Mater. 2021, 4, 12789−12797

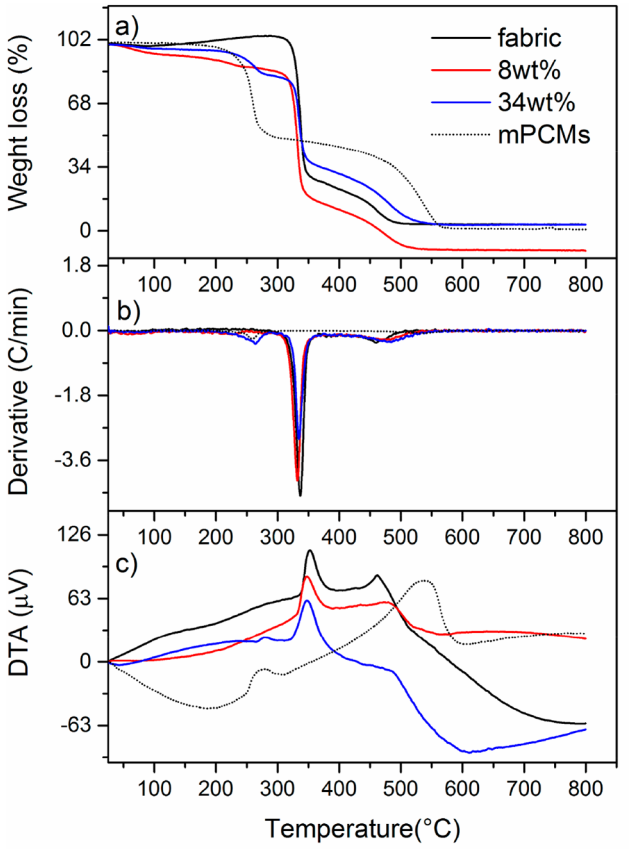

Figure 4. Thermogravimetric analysis measurements of impregnated and pure fabrics: (a) TG signal, (b) DTG signal, and (c) DTA signal.

docosane.[30] The fabrics impregnated with 8 wt % of mPCMs show a small decomposition step at about 24−242.3 °C total weight loss of 7 wt % due to water desorption. Then, the first main decomposition takes places at about 323.3−340.4 °C with a total weight loss of 65 wt % and the second one takes place in the range of 340.4−508.7 °C with a total weight loss of 28.3 wt %. The first main decomposition peak is related to the degradation of fabric matrix (very similar for TGA data of pure fabric) while the second demonstrates oxidation of the encapsulated docosane. It is interesting that no separate degradation peaks were observed for the shell of the embedded capsules, which indicates stabilization of the capsule shell of the fabric matrix, and the degradation of the capsule shell occurs in the same temperature range as for pure fabric. Fabrics impregnated with 34 wt % of mPCMs show a similar decomposition profile with a weight loss of 2.7 wt % and in the range of 88.8−234 °C. However, the first main decomposition takes place in the range of 234−272.4 °C with a total weight loss of 12.2 wt % associated with the degradation of the capsule shell not strongly bounded to the fabric fibers. The second one in the range of 272.4−342.3 °C that involves a loss of 46.2 wt % is associated with decomposition of the fabric and main part of the capsule shell, and the third one takes place at about 342.3−517.9 °C with a total weight loss of 33.9 wt %, demonstrating decomposition of encapsulated PCM. Table S1 contains TGA data with standard deviations. TGA weight losses can be also seen in the derivative signal (Figure 4b) that also shows a clear peak contributing to mPCMs as well as to fabrics impregnated with 34 wt % of mPCMs. This peak contribution appears much smaller for the fabrics with 8 wt % of mPCMs. The same tendency is observed in the DTA signal (Figure 4c); an exothermic process is observed at the same temperature interval for mPCMs and for the fabrics impregnated with 34 wt % mPCMs. The starting temperatures for the second and third main decomposition steps take place in the same temperature range as the first decomposition of the untreated fabric but also at the same temperature of the second decomposition of the mPCMs overlapping of processes.

We performed DSC measurements to determine the heat capacity of the impregnated structures. Figure 5 presents DSC

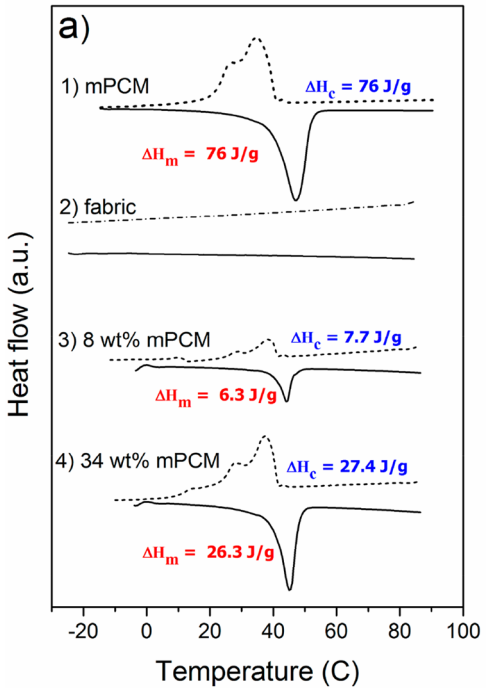

Figure 5. DSC thermograms for cotton fabric systems where (1) pure mPCMs, (2) untreated fabrics and loaded fabrics with (3) 8 wt % mPCMs and (4) 34 wt % mPCMs.

measurements for the pure fabrics and for fabrics with mPCMs. The mPCMs used for the impregnation of the fabrics have a melting temperature of T_m = 47.2 °C and melting enthalpy of ΔH_m = 76 J·g^{-1} on heating, while the crystallization temperature is centered at T_c = 34.6 °C with a shoulder at 26.5 °C, associated with a crystallization enthalpy of ΔH_c = 76 J·g^{-1} on cooling. Both heat uptake and release energy is the same, demonstrating stable heat uptake/release cycling.

The pure cotton fabrics exhibit no thermal events. DSC thermograms of the fabrics impregnated with 8 and 34 wt % of mPCMs show similar curves to those ones obtained for pure mPCMs which means the microcapsules attain latent heat capacity to the impregnated fabric network. The enthalpies of the impregnated fabrics increase with the increase of mPCMs wt % content. Impregnated fabrics with 8 wt % mPCMs show melting temperature T_m = 44.3 °C and melting enthalpy ΔH_m = 6.3 J·g^{-1} while the crystallization temperature and enthalpy are T_c = 37.6 °C and ΔH_c = 7.7 J·g^{-1}. There are several endothermic contributions during crystallization that take place above and below T_c at 43 °C (small peak contribution) and at 28 °C related to the different crystalline phases of n-docosane.[31,37,38] The fabrics impregnated with 34 wt %

https://doi.org/10.1021/acsaem.1c02170
ACS Appl. Energy Mater. 2021, 4, 12789−12797

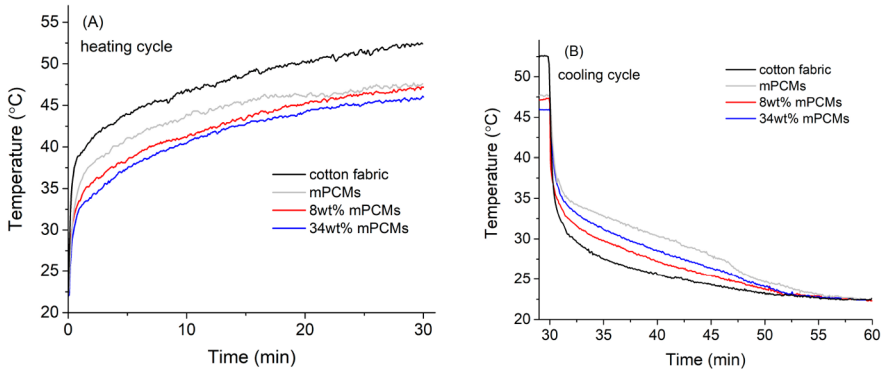

Figure 6. Dynamic heat storage measurements for (a) untreated cotton fabrics and treated cotton fabrics impregnated with 8 and 34 wt % of mPCMs, heating cycle; (b) untreated cotton fabrics and treated cotton fabrics impregnated with 8 and 34 wt % of mPCMs, cooling cycle. Results for pure mPCM are shown for comparison.

mPCMs show melting temperature and melting enthalpy T_m = 45.6 °C and ΔH_m = 26.3 J·g^{-1}, respectively, and a crystallization temperature and melting enthalpy T_c = 37 °C and ΔH_c = 27.4 J·g^{-1}, respectively. The obtained average latent heat values for the impregnated fabrics, ΔH_m = 6.3 J·g^{-1}, ΔH_c = 7.7 J·g^{-1} (8 wt %) and ΔH_m = 26.3 J·g^{-1}, ΔH_c = 27.4 J·g^{-1} (34 wt %) were used to calculate the mPCMs content resulting in 8.2 and 34.6 wt %, respectively, which is in accordance with the initial impregnation calculations for mPCM-fabric samples. Table S2 contains DSC data with standard deviations.

In the next step, we quantified the temperature reduction caused by the mPCMs in the fabrics by dynamic heat storage measurements (see Figure S4) that consisted of heating the samples up using an IR lamp (lamp on) for 30 min and then cooling them down (lamp off) for another 30 min with the measurements of temperature decrease FLIR T640 thermocamera. Figure S4 illustrates the setup for the dynamic heat storage measurements during the heating step: a thermocouple was connected to a recording system and placed in between two layers of the sample specimen and the surface temperature was recorded over time of the heating for 30 min. Cooling cycle (lamp was switched off for another 30 min) was monitored by FLIR T640.

Figure 6a shows the time-dependent temperature profiles for over 30 min of heating and cooling cycles for the impregnated fabrics with 8 and 34 wt % mPCMs and the untreated fabric used as a reference. The obtained curves for the heating cycles show a temperature gap for capsules' impregnated fabrics as compared with the pure one. In the beginning of the heating (1 min), the heating rate is fast. After several minutes at a temperature above the starting melting temperature of the n-docosane, $T_{m,onset}$ = 37 °C and within its phase change temperature range (37−45 °C) the heating rate is drastically lowered and temperature difference can be clearly seen between the capsules' impregnated fabrics and the untreated cotton fabrics. When PCM melting temperature is reached, the PCM is absorbing the heat during the phase change from solid to liquid state leading to a delay and reduction of the peak temperature. This temperature gap is still observed at the end of the heating cycle (until 30 min, Figure 6a). Fabrics with 8 wt % of mPCMs show considerable reduction of peak temperature of ∼5.2 °C compared to the untreated fabrics while the impregnated fabrics with 34 wt % of mPCMs showed 6.3 °C of temperature reduction. It is noticeable that impregnated fabrics with the highest mPCMs content of 34 wt % show a reduction in temperature of just 1.1 °C compared to the one with 8 wt % even though the content of microcapsules was 4 times higher.

The cooling cycles show similar energy saving efficiency for the composites impregnated with high quantity of the mPCM. Figure 6b demonstrates the cooling cycle for composites with the tendency for increasing thermal storage at a higher level of capsule impregnation. In the very beginning of the cooling (up to 1 min), the temperature drops abruptly with no clear difference between the samples because of the fast cooling rate. However, after 1 min of cooling, crystallization of PCM starts at about 36 °C and impregnated fabrics demonstrated higher temperatures than the ones without mPCM. After 7 min of cooling samples with high concentration of mPCM (34 wt % for textile fabrics) exhibited effective energy capacity keeping 10 °C temperature difference comparing to pure host materials. All samples went back to room temperature after 20 min of the cooling period (50 min of the heating/cooling cycle). The curve obtained for the pure mPCMs that was used also as reference (gray line), showing the mPCMs with the highest temperatures as well as the slowest temperature decrease due to the stored amount of heat that is being released during the cooling process.

DSC and dynamic heat storage measurements clearly demonstrate that when the mPCMs are heated they absorb the thermal energy equivalent to their heat capacity and undergo phase change transition from solid to liquid state which corresponds with the exothermic event in DSC (heating cycle). This phase change transition produces a reduction of the temperature increase when the mPCMs are present in the fabrics as a consequence of the PCM up-take of thermal energy. Reversibly, when the mPCMs are cooled down they release the previously stored heat while transitioning from liquid to solid state which corresponds to the endothermic peak in DSC (cooling cycle). This is in accordance to what has been observed in the dynamic heat storage measurements, that is, when the impregnated structures show higher temperatures than the pure structures due to the releasing of the heat.

The FTIR spectra were also obtained to determine whether the chemical nature of the impregnated fabrics was modified or not by their exposure to the IR source. As depicted in Figure 7, the impregnated fabrics show neither a peak modification nor decreased intensity. The process of up-taking and releasing of thermal energy by the mPCMs-impregnated structures is reversible and repeatable over a 100 cycles as we previously

https://doi.org/10.1021/acsaem.1c02170
ACS Appl. Energy Mater. 2021, 4, 12789−12797

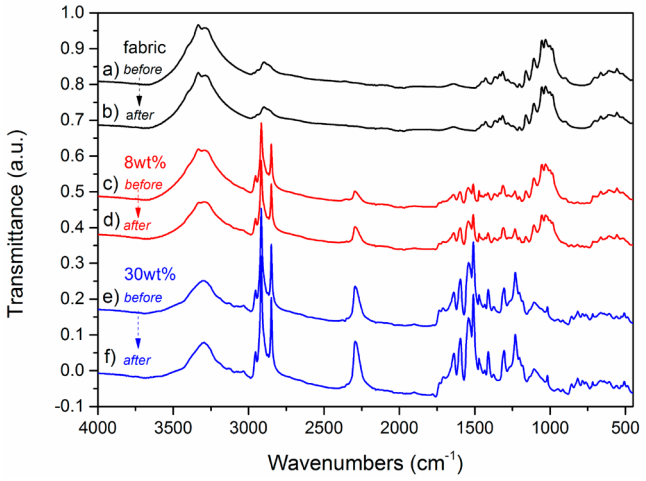

Figure 7. FTIR spectra (a,c,e) before and (b,d,f) after dynamic heat storage measurements for (a,b) pure fabrics, (c,d) fabrics impregnated with 8 wt % of mPCM, and (e,f) fabrics impregnated with 34 wt % of mPCM.

reported for highly stable PCM microcapsules for over a 100 heating and cooling cycles.[31]

Fabrics impregnated with 8 wt % of the mPCM showed almost similar heat capacity as fabrics impregnated with 34 wt % of the capsules; the same as for heating cycle. We continued our cycling and aging stability research with impregnated cotton fabrics samples with 8 wt % loading of mPCM to avoid overloading of the host material with capsules. Figure 8a demonstrates stability of the temperature control for fabrics impregnated with 8 wt % of the capsules. During the heating step, thermoregulating fabrics continuously keep about 11 °C temperature reduction for over 100 heating/cooling cycles. On the cooling step, fabrics with 8 wt % capsules retain approximately 6 °C temperature increase for over 100 cycles after switching off the heating source. This confirms sustainable effect of the incorporated capsules on the autonomic thermal response of the fabrics.

Moreover, we tested the energy saving efficiency of 4 years (1500 days) old fabrics with and without mPCM. Samples were stored at room temperature in the dark for more than 4 years and then their thermal uptake and release efficiency was tested (Figure 8b). At the heating step, pure aged fabric absorbed more heat leading to the increase of temperature by 3−4 °C comparing to the new fabric. The temperature of the aged fabrics with embedded capsules remained within the same range as for new samples (Figure 8a). As a result, the average temperature difference increased to about 14 °C but still remains stable for over 100 heating/cooling cycles. Similar observations were found for fabrics during the cooling step. An aged pure textile cooled down faster than new one with 2−3 °C temperature difference while the temperature of the fabrics with capsules did not change. The total temperature difference increased to 9 °C stable for over 100 cycles. Four years of storing fabrics with impregnated PCM capsules did not decrease heat control performance of the composite textile materials.

3. CONCLUSIONS

In summary, we impregnated cotton fabrics with n-docosane loaded polyurethane microcapsules (mPCMs) for thermal energy storage by simple dipping of the textile fabrics into the microcapsule suspension. We demonstrated the temperature control during heating and cooling of the modified textile fabrics stable for more than 100 heating/cooling cycles. We characterized the morphology, latent heat capacity, and thermoregulating properties of the impregnated structures. SEM images showed that mPCMs were successfully located inside textile network before and after 24 h washing in water.

Impregnated structures showed thermal stability up to 190 °C and high heat capacity. The observed heat capacity for fabrics impregnated with 8 wt % of mPCMs was 6.3 $J \cdot g^{-1}$ of the latent heat which provided 11 °C of temperature buffering effect during heating as compared to nonimpregnated fabrics for over 100 heating/cooling cycles, while the one with 34 wt % of mPCMs had 26.3 $J \cdot g^{-1}$ of latent heat and exhibited 12 °C temperature buffering. On the cooling step, impregnated fabrics demonstrated 6 °C temperature increase for over 100

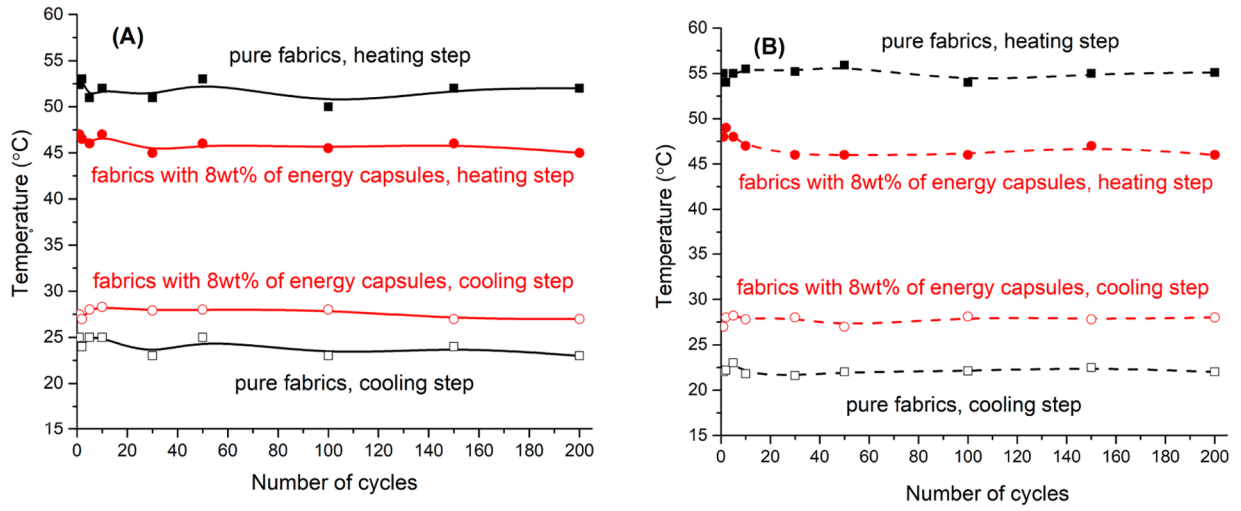

Figure 8. Cycling heat storage measurements for (a) freshly prepared, untreated cotton fabrics, and treated cotton fabrics impregnated with 8 wt % mPCMs at the 30th minute of the heating cycle and 10th minute of the cooling cycle; (b) 4 year old untreated cotton fabrics and treated cotton fabrics impregnated with 8 wt % mPCMs at the 30th minute of the heating cycle and the 10th minute of the cooling cycle.

https://doi.org/10.1021/acsaem.1c02170
ACS Appl. Energy Mater. 2021, 4, 12789−12797

cycles after switching off the heating source. Similar thermoregulating performance was observed for impregnated fabrics stored for 4 years at room temperature and ambient conditions. Temperature buffering effect increased to 14 °C during heating cycle and temperature increase effect reached 9 °C during cooling cycle. Both effects remained stable in aged fabrics. FTIR spectra showed no change in the chemical morphology after dynamic heat storage measurements indicating thermal and structural stability of the samples. Energy microcapsules are promising materials for various thermal-regulating applications including high-technical textiles, apparel, building materials, and paints.

4. EXPERIMENTAL SECTION

4.1. Microcapsule Preparation. The microencapsulated PCMs (mPCMs) were prepared by miniemulsion interfacial polymerization following the procedure previously developed by us.[30] PU shell was selected for their outstanding thermal stability and proven elasticity to overcome temperature and volume changes of the encapsulated PCM during heat uptake and release as confirmed in our previous studies.[39−41] Docosane was chosen as *n*-alkane because of its high heat capacity, noncorrosiveness and its transition temperature (T_m) of 37−40 °C suitable to be used in thermoregulating applications as functional textiles. The microcapsules have 2 μm size with melting and crystallization temperature (T_m and T_c) 47 and 35 °C, respectively, and melting and crystallization enthalpies (ΔH_m and ΔH_c) of 76 J·g^{-1}. Encapsulation yield was 77% of docosane (per capsule), which is close to theoretical capsulations considering shell thickness (79%). High elasticity of PU shell maintains integrity of the capsule load, as shown by DSC measurements.[31] The microcapsules were kept in water for their subsequent use for impregnation of fabrics. Resulting microcapsules have ∼3 ± 1 μm size.

4.2. Impregnation of the Fabrics. A plain weave white cotton fabric with unit weight of 100 g·m^{-2} (purchased from ZS Fabrics, U.S.A.) was selected as hosts to show the thermoregulating effect of the microencapsulated n-docosane in polyurethane shell. Impregnated fabrics with mPCMs were prepared by simple dipping of the cotton fabrics (1 cm^2) into 10 mL of the 8 or 32 wt % microcapsule solutions (prepared by dilution of initial 55 wt % capsule suspension in water) for 12 h under mild stirring followed by a drying step at 100 °C for 20 min in an oven and then cooling down to ambient conditions. This step was repeated with new microcapsule solutions until the desired impregnation concentration of microcapsules was achieved in the fabrics. Thermoregulatory properties are influenced by the mPCMs content in the fabrics; therefore, two different concentrations of the PCMs were studied: (1) the first one of about 8 wt % and (2) the second composition with higher content of mPCM of about 34 wt % to obtain textiles with higher energy storage capacity. The amount of mPCM in fabrics was experimentally measured by the ratio between melting enthalpy of fabrics with mPCM to the melting enthalpy of pure mPCM from DSC data.

4.3. Characterization. The morphology of the impregnated fabrics was determined using a JEOL JSM-7001F (Japan) scanning electron microscope (SEM). Samples were prepared by placing composite samples onto carbon tape on an aluminum SEM stub and further coating with chromium. Compatibility and adherence evaluation of the mPCMs to the fabrics were determined by immersing the impregnated structures into a water bath at 22 °C for 24 h and then examining by SEM.

Chemical characterization of the untreated and impregnated fabrics was done using Fourier transform infrared spectroscopy (FTIR) on a Bruker TENSOR II (Germany) instrument equipped with all reflective diamond ATR. Measurements were taken on transmittance mode with 64 scans from 400 to 4000 cm^{-1}.

Visual stability tests were carried out by heating the samples up to 50 °C, above the melting point of the PCM n-docosane for 30 min and leaving them to cool down. Photos were taken to follow the release of the PCM through the fabric structure.

Thermogravimetric analysis (TGA) experiments evaluated thermal stability and decomposition behavior of the fabrics. Thermogravimetric analysis was undertaken using a TGA STA PT1000 instrument from Linseis (Germany). Measurements were taken from room temperature up to 950 °C with a ramp of 10 °C·min^{-1} under air atmosphere and repeated three times for each sample.

Differential scanning calorimetry (DSC) was used to determine latent heat storage properties. DSC measurements were carried out in the range of −40 to 100 °C under nitrogen atmosphere with a 10 °C·min^{-1} ramp, using a DSC 204 F1 model from NETZSCH (Germany) and repeated three times for each sample.

Dynamic heat storage performance of the impregnated fabrics was evaluated by heating and cooling cycles from 20 to 55 °C using an IR lamp (150 W) to imitate solar radiation on the heating step. The heating/cooling cycles were carried out by switching on the IR lamp for 30 min and then switching off for another 30 min for the cooling cycles. The environmental temperature was 19 °C, and the dimensions of the sample specimens were 1.5 cm × 1.5 cm. For that purpose, a thermocouple sensor, with a resolution of 0.03 °C from 0 to 40 °C and of 0.1 °C from 40 to 100 °C, was placed in between the layers of the fabrics which was connected/plugged to a LABQUEST system from Vernier (U.S.A.) to record the time-dependent temperature profile and to measure temperature profile during heating. Temperature profiles during the cooling step were measured by FLIR T640 w/25° and 15° thermocamera (FLIR Systems Inc., U.K.) because of its high sensitivity during sample cooling. It is not possible to use FLIR instrument on the heating step because of the external heating exposure from IR lamp. Heat storage performance was measured in the cycling regime for fresh samples and 4 year old samples to demonstrate chemical and environmental stability of the mPCM incorporated into fabrics.

■ ASSOCIATED CONTENT

Supporting Information

The Supporting Information is available free of charge at https://pubs.acs.org/doi/10.1021/acsaem.1c02170.

Optical images of cotton fabrics impregnated with microencapsulated PCMs; SEM images of microPCM impregnated textiles after explosion to water for 24 h; heat transfer characteristics; setup for dynamic heat storage measurements (PDF)

■ AUTHOR INFORMATION

Corresponding Author

Dmitry G. Shchukin − *Gubkin University, 19991 Moscow, Russia; Stephenson Institute for Renewable Energy, University of Liverpool, Liverpool L69 7ZF, United Kingdom;* orcid.org/0000-0002-2936-804X; Email: d.shchukin@liverpool.ac.uk

Authors

Paula F. De Castro − *Leitat Technological Center, 08225 Barcelona, Spain*

Sergiy Minko − *Department of Chemistry, University of Georgia, Athens, Georgia 30602, United States;* orcid.org/0000-0002-7747-9668

Vladimir Vinokurov − *Gubkin University, 19991 Moscow, Russia*

Kirill Cherednichenko − *Gubkin University, 19991 Moscow, Russia*

Complete contact information is available at: https://pubs.acs.org/10.1021/acsaem.1c02170

Author Contributions

The manuscript was written through contributions of all authors. All authors have given approval to the final version of the manuscript.

Funding

ERC Enercapsule project (project 647969), NATO Science for Peace Program (project G5330), and RSF project (project 19-79-30091).

Notes

The authors declare no competing financial interest.

■ ACKNOWLEDGMENTS

We thank ERC Enercapsule project (project 647969), NATO Science for Peace Program (project G5330), and RSF project (project 19-79-30091) for funding this research.

■ REFERENCES

(1) Weinstein, L. A.; Loomis, J.; Bhatia, B.; Bierman, D. M.; Wang, E. N.; Chen, G. Concentrating Solar Power. *Chem. Rev.* **2015**, *115*, 12797−12838.

(2) Ma, T.; Yang, H.; Zhang, Y.; Lu, L.; Wang, X. Using Phase Change Materials in Photovoltaic Systems for Thermal Regulation and Electrical Efficiency Improvement: A Review and Outlook. *Renewable Sustainable Energy Rev.* **2015**, *43*, 1273−1284.

(3) Cardenas, B.; Leon, N. High Temperature Latent Heat Thermal Energy Storage: Phase Change Materials, Design Considerations and Performance Enhancement Techniques. *Renewable Sustainable Energy Rev.* **2013**, *27*, 724−737.

(4) Waqas, A.; Din, Z. U. Phase Change Material (PCM) Storage for Free Cooling of Buildings-A Review. *Renewable Sustainable Energy Rev.* **2013**, *18*, 607−625.

(5) Su, W.; Darkwa, J.; Kokogiannakis, G. Review of Solid-Liquid Phase Change Materials and Their Encapsulation Technologies. *Renewable Sustainable Energy Rev.* **2015**, *48*, 373−391.

(6) Wang, H.; Wei, Y.; Li, H. X.; Zhang, X. H.; Qi, H.; Tang, B.; Guo, Y. Y.; Ye, L. F.; Wang, H. Q. Octylammonium Sulfate Decoration Enhancing the Moisture Durability of Quasi-2D Perovskite Film for Light-Emitting Diodes. *Adv. Mater. Interfaces* **2021**, *8*, 2100442.

(7) Qu, Y.; Zhou, D.; Xue, F.; Cui, L. Multi-Factor Analysis on Thermal Comfort and Energy Saving Potential for PCM-Integrated Buildings in Summer. *Energy & Buildings.* **2021**, *241*, 110966.

(8) Borreguero, A. M.; Rodriguez, J. F.; Valverde, J. L.; Peijs, T.; Carmona, M. Characterization of Rigid Polyurethane Foams Containing Microencapsulted Phase Change Materials: Microcapsules Type Effect. *J. Appl. Polym. Sci.* **2013**, *128*, 582−590.

(9) Nomura, T.; Zhu, C.; Sheng, N.; Saito, G.; Akiyama, T. Microencapsulation of Metal-Based Phase Change Material for High-Temperature Thermal Energy Storage. *Sci. Rep.* **2015**, *5*, 9117.

(10) Zhao, C. Y.; Zhang, G. H. Review on Microencapsulated Phase Change Materials (MEPCMs): Fabrication, Characterization and Applications. *Renewable Sustainable Energy Rev.* **2011**, *15*, 3813−3832.

(11) Graham, M.; Shchukina, E.; De Castro, P. F.; Shchukin, D. Nanocapsules Containing Salt Hydrate Phase Change Materials for Thermal Energy Storage. *J. Mater. Chem. A* **2016**, *4*, 16906−16912.

(12) Graham, M.; Coca-Clemente, J. A.; Shchukina, E.; Shchukin, D. Nanoencapsulated Crystallohydrate Mixtures for Advanced Thermal Energy Storage. *J. Mater. Chem. A* **2017**, *5*, 13683−13691.

(13) Jin, Z.; Wang, Y.; Liu, J.; Yang, Z. Synthesis and Properties of Paraffin Capsules as Phase Change Materials. *Polymer* **2008**, *49*, 2903−2910.

(14) Su, J.; Ren, L.; Wang, L. Preparation and Mechanical Properties of Thermal Energy Storage Microcapsules. *Colloid Polym. Sci.* **2005**, *284*, 224−228.

(15) Yu, F.; Chen, Z.-H.; Zheng, X.-R. Preparation, Characterization, and Thermal Properties of microPCMs Containing n-dodecanol by using Different Types of Styrene-Maleic Anhydride as Emulsifier. *Colloid Polym. Sci.* **2009**, *287*, 549−560.

(16) Khakzad, F.; Alinejad, Z.; Shirin-Abadi, A. R.; Ghasemi, M.; Mahdavian, A. R. Optimization of Parameters in Preparation of PCM Microcapsules Based on Melamine Formaldehyde through Dispersion Polymerization. *Colloid Polym. Sci.* **2014**, *292*, 355−368.

(17) Rochmadi, A. P.; Hasokowati, W. Mechanism of Microencapsulation with Urea-Formaldehyde Polymer. *Am. J. Appl. Sci.* **2010**, *7*, 739−745.

(18) Sari, A.; Alkan, C.; Bicer, A.; Altuntas, A.; Bilgin, C. Micro/Nanoencapsulated n-nonadecane with Poly (Methyl Methacrylate) Shell for Thermal Energy Storage. *Energy Convers. Manage.* **2014**, *86*, 614−621.

(19) Wang, H.; Wang, J. P.; Wang, X.; Li, W.; Zhang, X. Preparation and Properties of Microencapsulated Phase Change Materials Containing Two-Phase Core Materials. *Ind. Eng. Chem. Res.* **2013**, *52*, 14706−14712.

(20) Sari, A.; Alkan, C.; Doguscu, D. K.; Bicer, A. Micro/Nano-Encapsulated n-heptadecane with Polystyrene Shell for Latent Heat Thermal Energy Storage. *Sol. Energy Mater. Sol. Cells* **2014**, *126*, 42−50.

(21) Fang, Y.; Kuang, S.; Gao, X.; Zhang, Z. Preparation and Characterization of Novel Nanoencapsulated Phase Change Materials. *Energy Convers. Manage.* **2008**, *49*, 3704−3707.

(22) He, F.; Wang, X.; Wu, Z. New Approach for Sol-Gel Synthesis of Microencapsulated n-octadecane Phase Change Material with Silica Wall using Sodium Silicate Precursor. *Energy* **2014**, *67*, 223−233.

(23) Yin, D.; Ma, L.; Liu, J.; Zhang, Q. Pickering Emulsion: A Novel Template for Microencapsulated Phase Change Materials with Polymer-Silica Hybrid Shell. *Energy* **2014**, *64*, 575−581.

(24) Borisova, D.; Mohwald, H.; Shchukin, D. G. Influence of Embedded Nanocontainers on the Efficiency of Active Anticorrosive Coatings for Aluminum Alloys Part II: Influence of Nanocontainer Position. *ACS Appl. Mater. Interfaces* **2013**, *5*, 80−87.

(25) Zheng, Z.; Schenderlein, M.; Huang, X.; Brownbill, N. J.; Blanc, F.; Shchukin, D. Influence of Functionalization of Nanocontainers on Self-Healing Anticorrosive Coatings. *ACS Appl. Mater. Interfaces* **2015**, *7*, 22756−22766.

(26) Fabien, S. In *The Manufacture of Microencapsulated Thermal Energy Storage Compounds Suitable for Smart Textile, Developments in Heat Transfer*; Dos-Santos-Bernardes, M. A., Ed.; InTech, 2011; Chapter 10.

(27) Song, C.; Duan, G. N.; Wang, D. J.; Liu, Y. F.; Du, H.; Chen, G. X. Study on the Influence of Air Velocity on Human Thermal Comfort under Non-Uniform Thermal Environment. *Building and Environment* **2021**, *196*, 107808.

(28) Khan, S.; Kim, J.; Acharya, S.; Kim, W. Review on the Operation of Wearable Sensors through Body Heat Harvesting Based on Thermoelectric Devices. *Appl. Phys. Lett.* **2021**, *118*, 200501.

(29) Mohaddes, F.; Islam, S.; Shanks, R.; Fergusson, M.; Wang, L.; Padhye, R. Modification and Evaluation of Thermal Properties of Melamine-Formaldehyde/n-eicosane Microcapsules for Thermoregulation Applications. *Appl. Therm. Eng.* **2014**, *71*, 11−15.

(30) Felix De Castro, P.; Shchukin, D. G. New Polyurethane/Docosane Microcapsules as Phase Change Materials for Thermal Energy Storage. *Chem. - Eur. J.* **2015**, *21*, 11174−11179.

(31) De Castro, P. F.; Ahmed, A.; Shchukin, D. G. Confined-Volume Effect on the Thermal Properties of Encapsulated Phase Change Materials for Thermal Energy Storage. *Chem. - Eur. J.* **2016**, *22*, 4389−4394.

(32) Nejman, A.; Gromadzinska, E.; Kaminska, I.; Cieslak, M. Assessment of Thermal Performance of Textile Materials Modified with PCM Microcapsules Using Combination of DSC and Infrared Thermography Methods. *Molecules* **2020**, *25*, 122.

(33) You, M.; Zhang, X. X.; Wang, J. P.; Wang, X. C. Polyurethane Foam Containing Microencapsulated Phase-Change Materials with Styrene-Divinybenzene Copolymer Shells. *J. Mater. Sci.* **2009**, *44*, 3141−3147.

https://doi.org/10.1021/acsaem.1c02170
ACS Appl. Energy Mater. 2021, 4, 12789−12797

(34) Zhu, Y.; Qin, Y.; Liang, S.; Chen, K.; Wei, C.; Tian, C.; Wang, J.; Luo, X.; Zhang, L. Nanoencapsulated Phase Change Material with Polydopamine-SiO_2 Hybrid Shell for Tough Thermo-Regulating Rigid Polyurethane Foam. *Thermochim. Acta* **2019**, *676*, 104−114.
(35) Zhang, W.; Hao, S.; Zhao, D.; Bai, G.; Zuo, X.; Yao, J. Preparation of PMMA/SiO_2 PCM Microcapsules and its Thermal Regulation Performance on Denim Fabric. *Pigm. Resin Technol.* **2020**, *49*, 491−499.
(36) Xiang, H.; An, J.; Zeng, X.; Liu, X.; Li, Y.; Yang, C.; Xia, X. Preparation and Properties of Polyurethane Rigid Foam Materials Modified by Microencapsulated Phase Change Materials. *Polym. Compos.* **2020**, *41*, 1662−1672.
(37) Sirota, E. B.; King, H. E.; Singer, D. M.; Shao, H. H. Rotator Phases of the Normal Alkanes: An X-ray Scattering Study. *J. Chem. Phys.* **1993**, *98*, 5809−5824.
(38) Kraack, H.; Sirota, E. B.; Deutsch, M. Measurements of Homogeneous Nucleation in Normal Alkanes. *J. Chem. Phys.* **2000**, *112*, 6873−6885.
(39) Costa, V.; Nohales, A.; Felix, P.; Guillem, C.; Gomez, C. M. Enhanced Polyurethanes Based on Different Polycarbonatediols. *J. Elastomers Plast.* **2013**, *45*, 217−238.
(40) Costa, V.; Nohales, A.; Felix, P.; Guillem, C.; Gutierrez, D.; Gomez, C. M. Structure-Property Relationships of Polycarbonate Diol-Based Polyurethanes as a Function of Soft Segment Content and Molar Mass. *J. Appl. Polym. Sci.* **2014**, *132*, 41704.
(41) Liu, K. K.; Williams, D. R.; Briscoe, B. J. Compressive Deformation of a Single Microcapsule. *Phys. Rev. E: Stat. Phys., Plasmas, Fluids, Relat. Interdiscip. Top.* **1996**, *54*, 6673−6680.

https://doi.org/10.1021/acsaem.1c02170
ACS Appl. Energy Mater. 2021, 4, 12789−12797